M Bassetti, A Belleri, A Marini. 2020. "Dynamic instability of axially loaded elements: general considerations and seismic loading". Journal of Constructional Steel Research, Vol. 170, pp.1-21
DOI: 10.1016/j.jcsr.2020.106088
Publisher's version at: https://doi.org/10.1016/j.jcsr.2020.106088

Dynamic instability of axially loaded elements: general considerations and seismic loading

Matteo Bassetti[1], Andrea Belleri[2], Alessandra Marini[3]
University of Bergamo, Department of Engineering and Applied Sciences

ABSTRACT

The phenomenon of dynamic instability of steel beams under harmonic axial loading is analysed, in particular to identify those elements in equilibrium under static axial loads, i.e. loaded below the Euler load, but that could fail under dynamic conditions, possibly compromising the entire structural stability. In the literature, the general problem of dynamic instability was comprehensively presented by Bolotin, who defined instability regions. Bolotin's method was extended herein and more accurate instability regions derived. In some conditions, depending on the ratio between the frequency of the exciting load and the beam transversal natural frequency, an elastic beam could sustain a dynamic axial load greater than the Euler load.

The influence of geometric and material non-linearity on the shape of the instability regions has been evaluated herein through time series analyses. Then, response spectrum analyses were conducted to highlight possible effects of dynamic instability due to seismic loading. Two building typologies were considered: multi-storey buildings with cross bracing and existing industrial buildings. The results show that in the case of elements of the bracing system of new-designed multi-storey buildings, the dynamic instability is generally not an issue due to the high frequency of the single elements compared to the frequency of the fundamental mode of vibrations of the whole building. In the case of existing industrial buildings not designed to sustain seismic actions, some slender elements, with frequency of vibration compatible with the fundamental frequencies of the building, may undergo dynamic instability with possible detrimental effects in the whole building response.

Keywords: dynamic instability; seismic action; axially loaded beams.

[1] Research grant holder
[2] Associate professor, corresponding author: andrea.belleri@unibg.it
[3] Associate professor

1. INTRODUCTION

The stability of elements subjected to static and dynamic loading conditions has been widely studied over the years, particularly during the last century [1] [2] [3] [4] [5] [6] [7]. Among these topics, the phenomenon of dynamic instability is investigated herein.

When an elastic beam is subjected to a periodic axial load, whose amplitude is less than the Euler critical load, the beam will in general show only longitudinal vibrations. However, for some combinations of the ratio between the loading frequency and the transverse vibration frequency of the beam, the element will experience transverse oscillations with increasing amplitude, i.e. instability occurs. This phenomenon is known as dynamic instability and, although being extensively analysed in the context of mechanical and aerospace engineering, particularly for plates [8] [9] [10] [11] [12], it has not been systematically applied in the field of seismic engineering. In this scenario, the purpose of this work is to analyse the dynamic instability of steel elements, both in the elastic and inelastic range, and to define a method for its evaluation in the case of seismic loading by means of a response spectrum analysis.

The general theory of dynamic instability was comprehensively presented in Bolotin (1964) [13], who provided solutions to engineering problems using simplified mathematical methods by which he introduced the concept of "instability regions" as those regions in which dynamic instability may occur, i.e. indefinitely increasing transverse vibration of an axially loaded beam, as opposed to the "safe regions" where no instability is expected. Bolotin provided an approximation of the instability regions for elastic, simply-supported, constant cross-section beams as a function of the loading frequency, the transverse frequency of the beam, the initial loading conditions and the amplitude of the harmonic excitation. The small displacement-small deflection assumption applies. Other applications of this theory regard rods subjected to axial jump loading, where axial vibrations give rise to periodic axial loads which in turn cause unstable bending vibrations [14] [15], and the influence of wind loads in the elements of a building type structure [16]. An interesting application in the field of earthquake engineering was carried out by Azad et al. [17], who studied the effects of seismic loading on braced steel frames by means of non-linear dynamic analysis. In particular, the overload recorded in the braces and the frequency for which the phenomenon occurred were analysed. After evaluating the effect of this overload on the adjacent elements, a method was proposed to account for the overload in the design stage. For the treatment of dynamic instability equations and problems the use of a finite element approach is nowadays widely adopted [9] [11] [16] [17] [18].

In this study the method for determining the regions of dynamic instability proposed by Bolotin [13] has been extended to derive more accurate instability regions. The influence of geometric and material non-linearity and of the beam slenderness on the distribution of unstable regions was evaluated by means of non-linear dynamic analyses. It is interesting to note that, in some conditions, the beam could sustain a dynamic axial load greater than the Euler instability load. Such conditions could affect the application of the capacity design for earthquake type loading.

The possibility of dynamic instability in building type structures was investigated by means of response spectrum analyses considering two case studies: a steel multi-storey building with cross-bracing designed to sustain seismic actions and a single-storey industrial building not designed for seismic actions. The results show that in the former case the dynamic instability is not an issue: in the cross-bracing elements there are no cases where the axial load exceeds the static instability load therefore capacity design is not affected; in the columns of the bracing system there are no cases where dynamic instability occurs for lower than expected axial loads. This is due to the high frequency of vibration of the single elements compared to the frequency of the fundamental mode of vibrations of the whole building. In the latter case, existing industrial buildings not designed to sustain seismic actions, some slender elements, with frequency of vibration compatible with the fundamental frequencies of the building, may undergo dynamic instability with possible detrimental effects in the whole building response.

2. THEORY OF DYNAMIC INSTABILITY

Considering the transverse oscillations of a simply-supported beam with no geometric imperfections subjected to a periodic axial load (**Figure 1**), the differential equation governing the problem in the case of small deflection [13] is:

$$EJ\frac{\partial^4 v}{\partial x^4} + P\frac{\partial^2 v}{\partial x^2} + m\frac{\partial^2 v}{\partial t^2} = 0 \qquad (1)$$

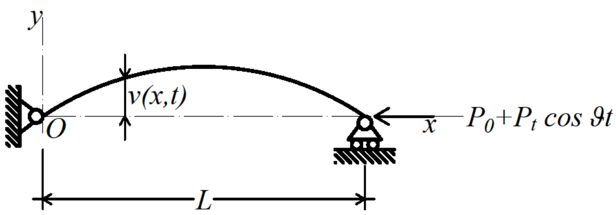

Figure 1: Deformed configuration of a straight rod loaded with a longitudinal periodic load.

where EJ is the beam bending stiffness, P is the longitudinal force defined as $P(t) = P_0 + P_t \cos \vartheta t$, ϑ is the frequency of the load and m is the mass per unit length of the beam. The solution of Eq. (1) is sought in the form:

$$v(x,t) = f_k(t)\,\sin\frac{k\pi x}{L} \qquad (k = 1, 2, 3, \dots) \qquad (2)$$

where $f_k(t)$ are unknown functions of time and L is the length of the rod. Replacing Eq. (2) into Eq. (1) it yields:

$$\left[m\frac{\partial^2 f_k}{\partial t^2}+EJ\frac{k^4\pi^4 f_k}{L^4}-(P_0+P_t\cos\vartheta t)\frac{k^2\pi^2 f_k}{L^2}\right]\sin\frac{k\pi x}{L}=0 \qquad (3)$$

To satisfy this equation, the expression contained in the square brackets must be zero. The new expression obtained is the same for all k, which therefore will be omitted for sake of clarity.

It is convenient to define the following parameters:

- the angular frequency of the first mode of transverse vibrations of the unloaded beam:

$$\omega=\frac{\pi^2}{L^2}\sqrt{\frac{EJ}{m}} \qquad (4)$$

- the angular frequency of the first mode of transverse vibrations of the beam loaded by a constant longitudinal force P_0:

$$\Omega=\omega\sqrt{1-\frac{P_0}{P_e}} \qquad (5)$$

- the Euler critical load:

$$P_e=\frac{\pi^2}{L^2}EJ \qquad (6)$$

- the excitation parameter:

$$\mu=\frac{P_t}{2(P_e-P_0)} \qquad (7)$$

It is interesting to note that $\mu = 0.5$ leads to $P_t + P_0 = P_e$, therefore to the Euler critical load for static conditions. Introducing these parameters in Eq. (3), one obtains:

$$f''+\Omega^2(1-2\mu\cos\vartheta t)f=0 \qquad (8)$$

where f'' is the second derivative of f with respect to time. This second-order homogeneous linear differential equation is known as Mathieu-Hill equation [19] [20]. Finally, by introducing in Eq. (8) the damping term ε, defined as:

$$\varepsilon=\xi\Omega \qquad (9)$$

where ξ is the relative damping, the following differential equation is obtained:

$$f''+2\varepsilon f'+\Omega^2(1-2\mu\cos\vartheta t)f=0 \qquad (10)$$

Such equation could be related to a Mathieu-Hill equation and its solution is reported in the **Appendix A**. Bolotin [13], by considering only 2x2 systems of equations, provided closed-form solutions on the problem and identified the boundaries of regions of dynamic instability in the plane ($\vartheta/2\Omega$, μ). It is worth noting that some regions exist in which stability is guaranteed for axial loads exceeding the Euler critical load.

To refine the results obtained by Bolotin [13], the systems of equations were extended considering a matrix size 8x8 and 7x7 respectively (**Appendix A**) and solved analytically. The boundaries of the first 3 dynamic instability regions obtained from the refined solution (8x8 matrix for region 1 and 3, and 7x7 matrix for region 2) are compared to the boundaries obtained from less refined solutions, i.e. 4x4 matrix and 2x2 matrix, being the latter solution the one adopted by Bolotin [13]. **Figure 2** shows this comparison for both the non-damped and damped case ($\xi = 1\%$). It is observed that the instability regions obtained from the simplified method (referred to as "Bolotin" in **Figure 2**) [13] represent a reasonable approximation of the solution up to $\mu = 0.5$, while for higher values of μ a significant difference is observed, especially for the lower boundary of each region. Looking at the overall results presented in **Figure 3**, i.e. at all the seven instability regions, it is observed how the instability regions for $\vartheta/2\Omega$ approaching 0 (i.e. for quasi static loading) tend to $\mu = 0.5$, i.e. to the Euler critical load. Another interesting aspect is that between the first pairs of regions (i.e. between the 1st and the 2nd region and between the 2nd and the 3rd region) it is observed how stable solutions are possible when P_0 is lower than the Euler critical load (P_e) but the total loading ($P_0 + P_t$) exceeds P_e. This aspect was not highlighted in the previous formulation [13]. From **Figure 3** it is evident that damping involves a shift to the right of the origin of the instability regions. Furthermore, an attempt to define simplified regions in which dynamic instability does not occur is reported in **Appendix B**.

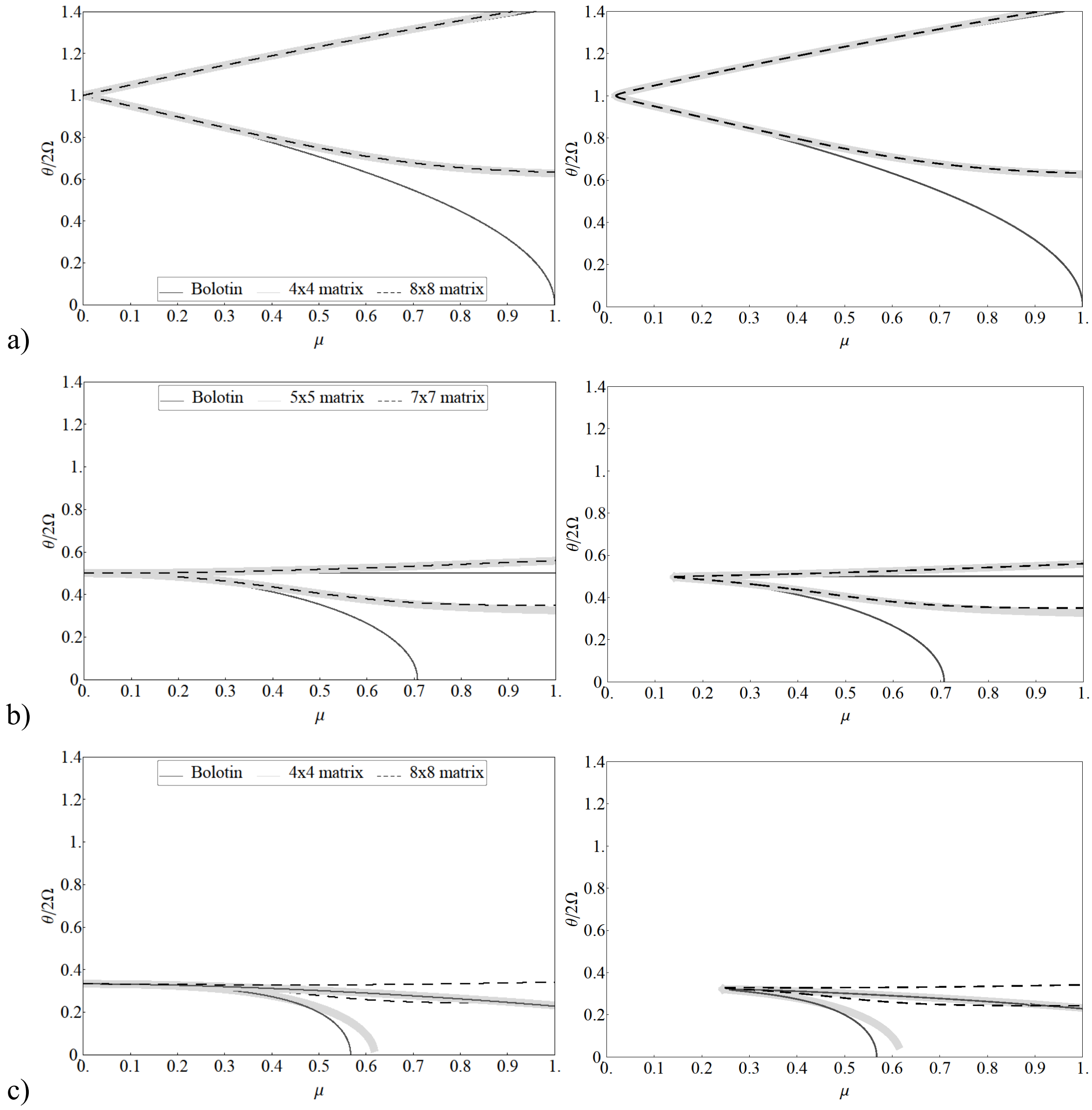

Figure 2: Comparison of the boundaries of the first three regions of dynamic instability investigated by Bolotin.

Note: a), b), and c) correspond to the 1st, 2nd, and 3rd region of instability.

Left-side undamped case, right-side damped case ($\xi = 1\%$).

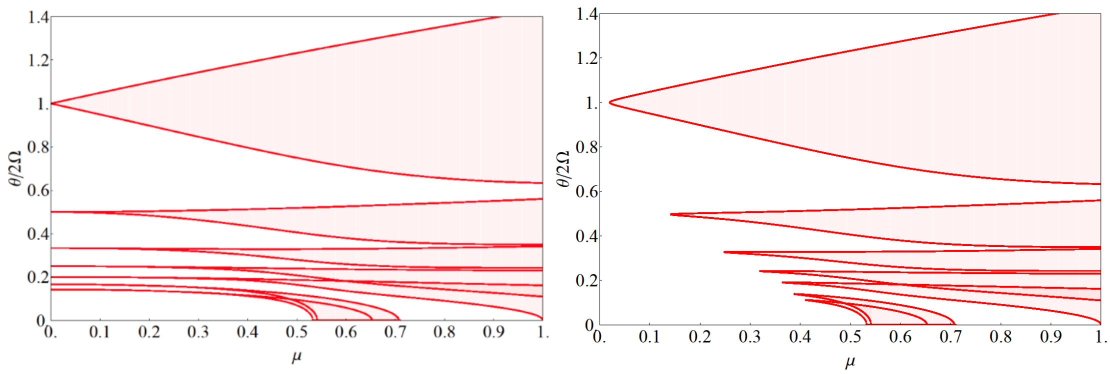

Figure 3: Regions of dynamic instability obtained from the 8x8 matrix and 7x7 matrix.

Note: left-side undamped case, right-side damped case, $\xi = 1\%$.

3. INFLUENCE OF NON-LINEARITIES

The previous considerations are based on the hypotheses that the beam is perfectly linear, the material is elastic and the small-displacements assumption applies. This section investigates the possible variation of the shape of the instability regions by removing the hypothesis of small-displacements and by including an initial imperfection of the beam and the non-linearity of the material, i.e. considering the plastic properties of the steel. Subsequently, another slenderness ratio was analysed. To account for all these sources of non-linearity, a series of numerical time history simulations has been conducted for various conditions ranging in the previously considered extensions of the μ - $\vartheta/2\Omega$ plane. The finite element software Abaqus [21] and the Abaqus2Matlab [22] toolbox were used to automate the process in a Matlab [23] environment to extract the value of the transverse oscillation of the beam and the moment-curvature relationship at mid-span.

A starting model was created in Abaqus [21] and its properties modified to perform the different series of analysis. Such model consists of a steel beam (grade S235) of length L equal to 4 m, with a constant circular cross-section of diameter D, constrained at one end by a perfect hinge, while at the other end by a simple support allowing the translation along the beam axis direction. An initial sinusoidal imperfection was assigned to the beam, which was subdivided into ten segments (**Figure 4**).

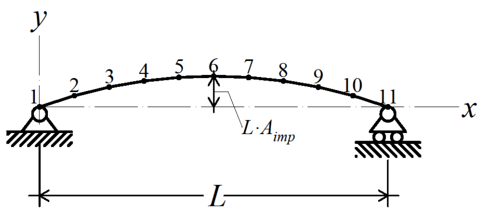

Figure 4: Considered finite element model with initial geometry imperfection.

Starting from this model, other models were derived with the characteristics shown in **Table 1**. The influence of the initial geometry imperfection was investigated with model A, for increasing amplitude of the initial imperfection, the evaluation of the material non-linearity with model B, by introducing the plastic properties of the material, and the influence of the slenderness with model C. The beam instability was evaluated considering the exceedance of a transverse displacement at the mid-span equal to 1/50 of the beam length L. Such limit was selected, for demonstration purposes, based on the following considerations: L/50 corresponds to 10 times the standard initial imperfection (L/500) and it also corresponds to 5 times the lateral displacement associated with an axial load corresponding to the critical load, considering elastic conditions and a first order analysis. In addition, higher deflections may trigger damage in the connections. From a computational point of view such a limitation helped in reducing the analysis time. Other limit values may alternatively be selected without compromising the general results presented herein. Regarding the time duration of each analysis, a total time of 1s, 3s and 10s was considered to evaluate the influence of the duration of loading on the onset of dynamic instability: indeed, Bolotin [13] referred to the dynamic instability triggered by a stationary sinusoidal signal, while earthquakes are non-stationary events. It is worth observing that the 10s duration leads to an approximation of the boundaries of the instability regions comparable with the results of the extensions of Bolotin method [13] highlighted in the previous section.

The nonlinear properties of the steel are included by means of a piecewise linear stress-strain relationship passing through the following points: (0; 0), (235 MPa; 0.001119), (360 MPa; 0.076119), (235 MPa; 0.131119), (100 MPa; 0.201119). Abaqus B21 elements ("Beam" element with linear interpolation in the plane) with a mesh size 0.4m were used, but for the segments 5-6 and 6-7 of the elasto-plastic model a mesh size of 0.1m were considered. Furthermore, a Rayleigh damping was included in the model calculated by considering a relative damping $\xi = 1\%$ for the 1st and 3rd transverse modes of vibration.

Table 1: Characteristics of the considered FE models.

Note: D is the beam dimeter; λ is the normalized slenderness; ω is the natural angular frequency of the beam; P_e is the Euler critical load; P_{pl} is the elasto-plastic load (evaluated by means of a quasi-static pushover analysis).

Model	Material	D (m)	λ	ω (Hz)	P_e (kN)	P_{pl} (kN)
A	Linear Elastic	0.0875	1.9471	11.1	372.7	-
B	Elasto-Plastic	0.0875	1.9471	11.1	372.7	307.6
C	Elasto-Plastic	0.1750	0.9735	22.2	5963.8	3542.0

The characteristics of the considered models are summarized in **Table 2**. The amplitude, P_t, and the angular frequency, ϑ, of the harmonic external load were varied to cover the μ - $\vartheta/2\Omega$ plane with sufficient accuracy, i.e. variations of μ and $\vartheta/2\Omega$ equal to 0.0116 and 0.0242 respectively.

The results of the analyses are reported in the following graphs in which the dynamically unstable points ($\mu, \vartheta/2\Omega$) are plotted with the symbol *. Moreover, the following graphs show the boundaries of the instability regions previously determined (with red continuous lines), the value for which the sum between the initial load P_0 and the variable load P_t is equal to the Euler critical load P_e (i.e. $\mu = 0.5$, with a blue continuous line), and the value for which the sum between the initial load P_0 and the variable load P_t is equal to the maximum plastic load P_{pl} evaluated under static conditions (with a blue dotted line).

Table 2: Parameters considered in each analysis series.

Note: A_{imp} is the ratio between the amplitude of the initial imperfection and the beam length.

Id.	**Model**	A_{imp}	P_0 **(kN)**	P_0 / P_e	P_0 / P_{pl}
A1	A	l/1000	50.0	13.4%	-
A2	A	l/500	50.0	13.4%	-
A3	A	l/250	50.0	13.4%	-
B1	B	l/500	0	0 %	0 %
B2	B	l/500	50.0	13.4%	16.3%
B3	B	l/500	186.5	50.0%	60.6%
B4	B	1/500	228.1	61.2%	74.2%
B5	B	l/500	260.0	69.8%	84.5%
C1	C	l/500	575.7	9.6%	16.3%

The influence of the geometric non-linearity is shown in **Figure 5**. It is worth noting that the greater the analysis time, the better the approximation of the instability regions for all the series. In addition, it is observed that the bounds are affected by the duration of analysis, particularly for low values of μ (i.e. low initial load and low dynamic load). For this condition, the increase of the lateral displacement during dynamic loading occurs at a slower rate. Moreover, if the initial imperfection increases, from series A1 to A2 and to A3, the number of unstable cases increases in the case of $\vartheta/2\Omega$ values lower than 0.5; such unstable points are characterised by μ values lower than those theoretically predicted (i.e. a left shift of the instability regions). The geometric non-linearity does not affect the solution only for the 1st region of instability, as the unstable cases are almost identical for all the series and in accordance with the theoretical formulation. It is observed that a portion of the plane between the 1st and 2nd instability region is characterized by a stable response for μ values greater than 0.5 (i.e. greater than the Euler critical load). Finally, it is observed that in the case of static loading (i.e. $\vartheta/2\Omega = 0$), the onset of instability is related to the considered maximum lateral deflection taken as reference (herein 1/50 of L): indeed, the greater the initial imperfection, the lower the load (and therefore μ) required to reach such lateral deflection.

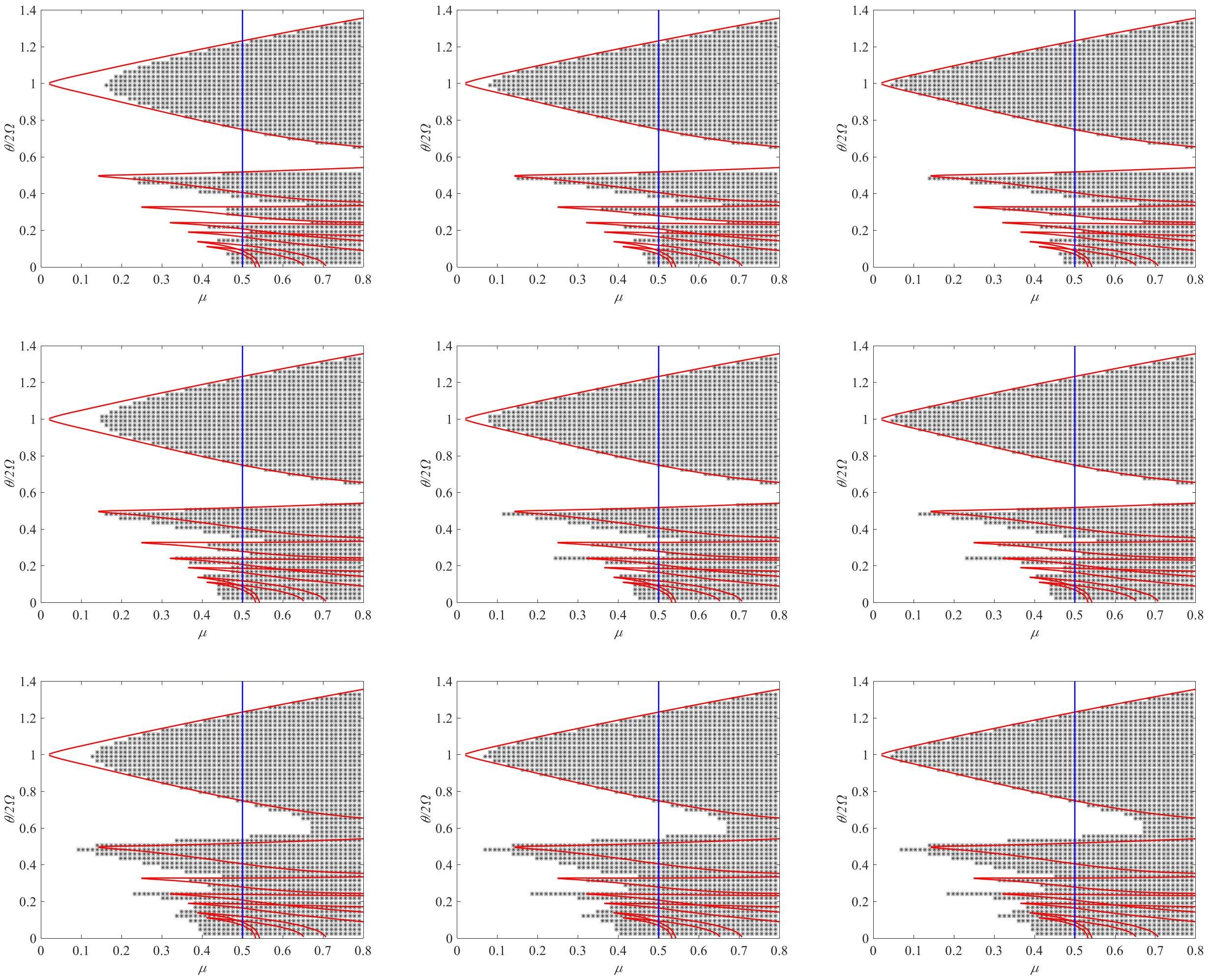

Figure 5: Results of model A: investigation of geometric non-linearity (series A1, A2, and A3 from top to bottom) for different durations of the analysis time (1s, 3s, and 10s from left to right).

Figure 6 shows the results obtained from the investigation of the influence of the material non-linearity, obtained from introducing the plastic characteristics of the steel. As in the elastic case, it is observed that the number of unstable points in the analysis increases with the increase of the analysis time. The 1st region of instability is similar in the elastic and inelastic case, while for the higher order regions the unstable cases are outside the theoretical boundaries and they are characterized by lower values of μ (i.e. a left shift of the instability regions). This aspect is more pronounced with the increase of the initial load P_0. It is observed that all the additional unstable points found in the inelastic case are characterized by inelastic transverse vibrations: i.e. the load demand in the rod (axial load and bending moment due to the 2nd order effects) for elastic conditions leads to stress values exceeding the yield stress, therefore in the inelastic case yielding occurs; under these conditions the system becomes dynamically unstable after introducing the material non-linearity. Finally, it is worth noting that between the 1st and 2nd instability regions there are still stable points beyond the axial capacity of the beam.

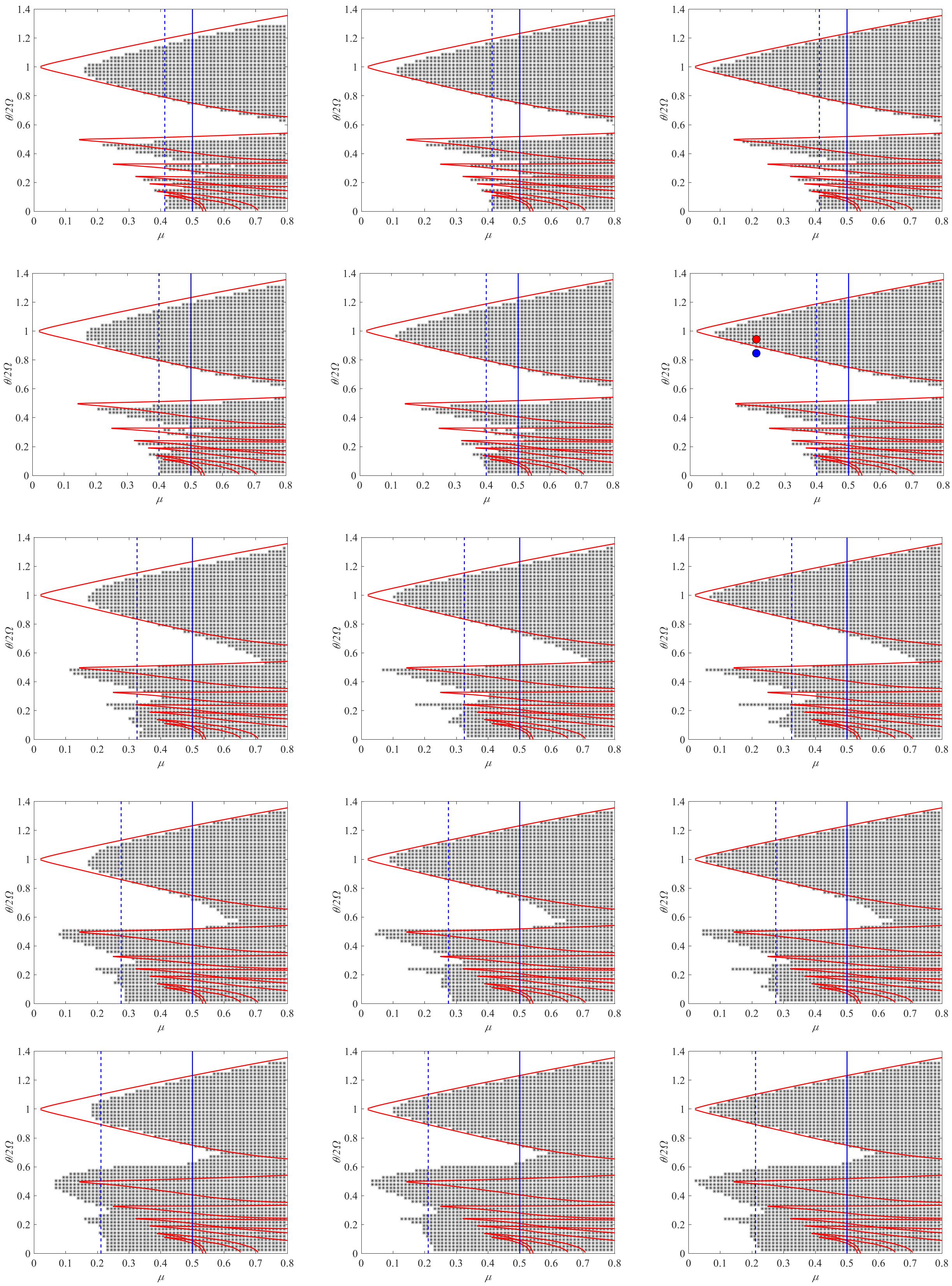

Figure 6: Results of model B: influence of material non-linearity (series B1, B2, B3, B4, and B5 from top to bottom) for different durations of the analysis time (1s, 3s, and 10s from left to right).

For sake of clarity, the time history of a stable and an unstable point across the boundary of the 1st region of instability (blue and red circles in **Figure 6**, respectively) are reported in **Figure 7** in the case of plastic (**Figure 7a**) and elastic (**Figure 7b**) material.

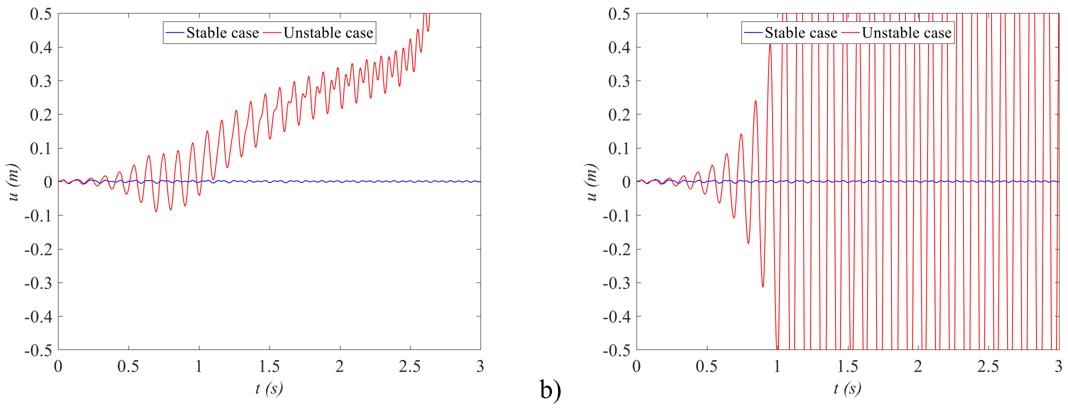

a) b)

Figure 7: Time history of a stable (blue circle) and an unstable (red circle) point of series B2 (**Figure 6**) in the case of **a)** plastic material and **b)** elastic material.

Figure 8 shows the comparison between the results of the series C1, selected to assess the influence of the beam slenderness λ ($\lambda_C = 0.5\ \lambda_B$), and the results of the series B4, since both cases are characterised by the same μ value for static conditions (i.e. for $\vartheta/2\Omega = 0$). The unstable points of the two series are represented with an empty circle and with a filled circle, respectively. As for the previous investigations, if the analysis time increases, the number of unstable points also increases. It is observed that the results of series C1 are all unstable beyond the continuous blue line (i.e. the sum between the initial load P_0 and the variable load P_t is equal to the Euler critical load) and, generally, unstable points are found for μ greater than 0.4 between the 1st and 2nd regions and above the 1st region. This is associated with the difference of lateral deflection at yielding of the two series: series C1 is characterized by yielding at the midspan cross-section for a much smaller lateral deflection compared to series B4, 0.009m compared to 0.031m respectively. Considering the additional unstable points of series C1, i.e. for instance the points between the 1st and 2nd instability regions, the lateral deflection demand in the case of elastic material is much larger than the displacement associated with yielding in the case of plastic material, i.e. far beyond 0.009m. This comparison is shown in **Figure 9** in terms of time history for the blue circle depicted in **Figure 8** for series B4 and C1 for both elastic and plastic material. Considering the reduction of unstable points in the 2nd region (**Figure 8**), it is worth noting that such behaviour is not related to the time of analysis, but to a peculiar combination of plasticity and loading frequency which needs to be further investigated.

Similar results for models A, B, and C are obtained from considering 3% of relative damping as reported in **Appendix C** along with a close up of the results in the plane (μ; $\vartheta/2\Omega$) between (0; 0) and (0.5;0.6). In that case the designer could directly enter the provided graphs with the (μ; $\vartheta/2\Omega$) point corresponding to a specific element and loading conditions and determine the possibility of dynamic instability.

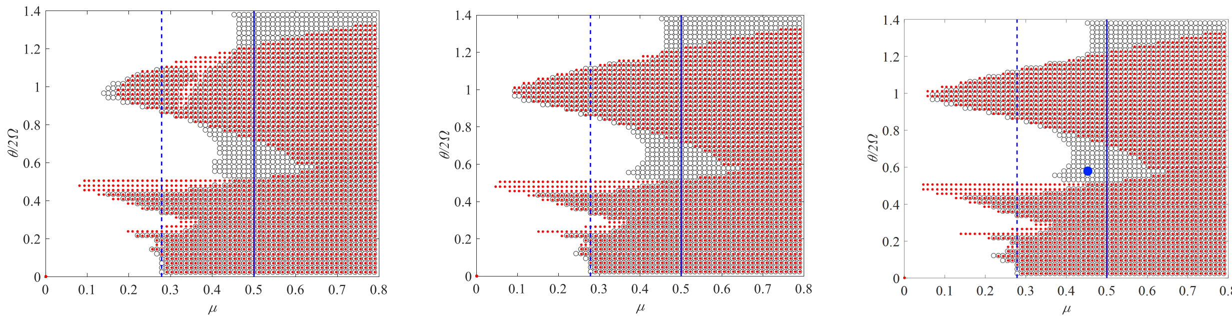

Figure 8: Results of model C: investigation of the influence of the slenderness ratio (series C1) for different durations of the analysis time (1s, 3s, and 10s from left to right).

Note: the empty and filled circles are the unstable points of series C1 and B4 respectively

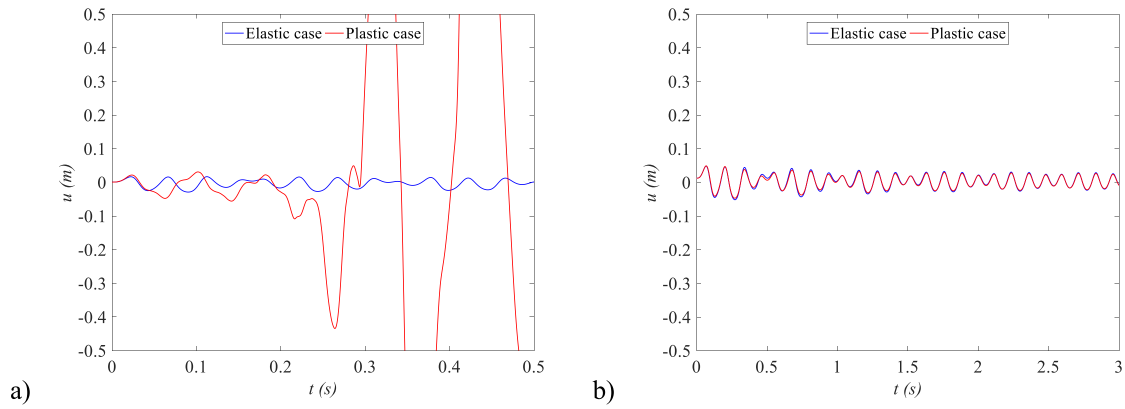

Figure 9: Time series of a reference point (blue circle) of **Figure 8** in the case of **a)** series C1 and **b)** series B4.

4. DYNAMIC INSTABILITY DUE TO SEISMIC LOADING

Possible onset of dynamic instability in building type structures due to seismic loading could be directly evaluated in the design phase by means of response spectrum analysis, which is a linear dynamic approach based on the decoupling of the fundamental modes of vibration in classically damped systems. Given a building, and in general a multi degree of freedom (MDOF) system, the elastic response, for instance in terms of displacements and internal actions, may be directly obtained from adding the response of single degree of freedom (SDOF) systems which represent the fundamental modes of vibration of the original structure (**Figure 10**). Each of these SDOF systems is characterized by a modal participation factor which acts as a weight for the total response. More details can be found for instance in [26].

Given these premises, it is possible to introduce the response spectrum analysis, which measures the contribution of each natural mode of vibration to the seismic response of a MDOF system. A response spectrum collects the maximum response of SDOF systems with different periods of vibration (**Figure 10**), for instance in terms of acceleration or displacement, when they are subjected to the same ground motion. Considering a building and its fundamental modes of vibration, it is possible to evaluate the maximum acceleration of each of them in the response spectrum and to combine them to find the overall likely maximum response of the MDOF system. Various combination techniques maybe adopted to account for the non-contemporaneity of the maximum values of the SDOF systems, such as the square-root of the sum of the square rule [26]. Finally, to account for the inelastic behaviour of the system, the building codes introduce a behaviour factor, which is a function of the structural typology, to reduce the ordinate values of the response spectrum.

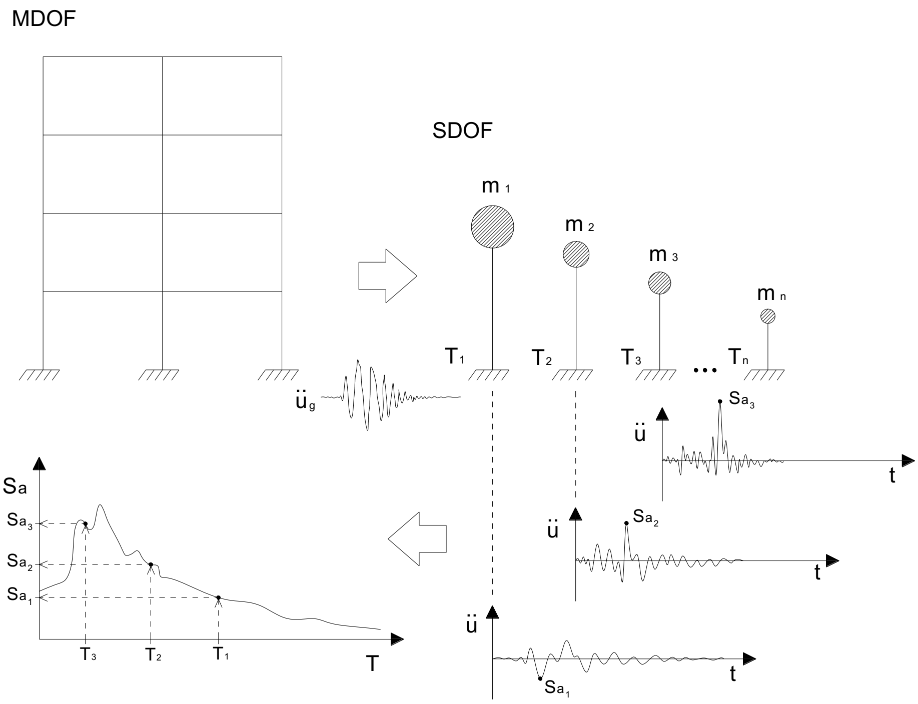

Figure 10: Scheme of response spectrum analysis.

Note: T_i and m_i are the period of vibration and participation mass of the i[th] SDOF system, respectively; Sa_i is the maximum acceleration of the i[th] SDOF system under a ground acceleration $\ddot{u}_g$.

In the present study, the contribution of the various vibration modes is accounted for by considering single modes at a time in the analysis: for instance, carrying out a response spectrum analysis taking into account the sole 1st mode of vibration allows obtaining the variation of the axial load in the elements (i.e. P_t according to the previous formulation) associated with the 1st mode of vibration of the system, which is characterized by a specific angular frequency (i.e. ϑ according to the previous formulation, therefore the frequency of load). Once P_0, P_t, and ϑ have been defined, it is possible to evaluate the dynamic instability of each axially loaded beam, which is characterized by a transverse angular frequency Ω, following the formulation presented in the previous sections. Similar considerations apply for the evaluation of possible dynamic instability in the case of higher order modes of vibration. It is worth noting that the use of a response spectrum analysis provides results on the safe side because the values of such analysis are associated with the maximum values experienced by the system during the earthquake.

At this regard two case studies have been considered: a cross-braced multi-storey building (4 and 11 storeys) designed for seismic actions and an existing single-storey industrial building not designed for seismic actions. Each case study was subjected to response spectrum analyses, with the software MidasGEN [24], considering a design spectrum corresponding to the life safety limit state in accordance to Eurocode 8 [25] with soil class B, ground acceleration on rock a_g equal to 0.270g, relative damping equal to 5%. The analyses were conducted considering a behaviour factor (q) equal to 4, i.e. in accordance with Eurocode 8 [25] for concentrically braced frames, in the first case study, and equal to 1.5, i.e. referring to existing industrial buildings not specifically designed for seismic loading, in the second case study.

4.1. Case study 1: multi-storey building

The case study shown in **Figure 11** was selected as representative of cross-braced buildings designed for seismic actions. The response spectrum analysis of the whole building was considered and the effects of dynamic instability in the elements of the bracing system (columns and diagonals) were evaluated. For both the 4 and 11 storeys cases, the columns and the beams are made by HEM400 and HEA300 profiles respectively. Moreover, the columns of the ground floor of the 11 storeys building are made by HEM600. Pinned connections are considered between the elements. The steel grade is S355 and the floor tributary mass is 71800kg. The diagonal elements, 5.83m long, are considered unloaded due to gravity (i.e. $P_0 = 0$) and were designed based on the tension load resulting from a response spectrum analysis.

Considering that the Eurocode 8 [25] prescribes that the non-dimensional slenderness, $\bar{\lambda}$, must be limited between 1.3 and 2.0, a parametric analysis was carried out to evaluate the influence of $\bar{\lambda}$ on the distribution of points in the μ - $\vartheta/2\Omega$ plane. At this regard, multiple analyses were carried out by varying the steel profile of the diagonal elements in each analysis, therefore varying the values of $\bar{\lambda}$ and the working rates (**Table 3**). Among these, the profiles allowed by Eurocode 8 [25] are HEA140, HEA120, HEA100 and 2L90x90x6. The excitation coefficient (μ) (Eq. (7)) and the frequency ratio ($\vartheta/2\Omega$) were calculated after obtaining the load due to the earthquake (P_t) from the response spectrum analyses. The resulting points for the diagonal elements of each floor level are represented in **Figure 12**: the increase of the non-dimensional slenderness leads to an increase of both the frequency ratio and of the excitation coefficient. The latter is associated with the decrease of the Eulerian critical load (P_e).

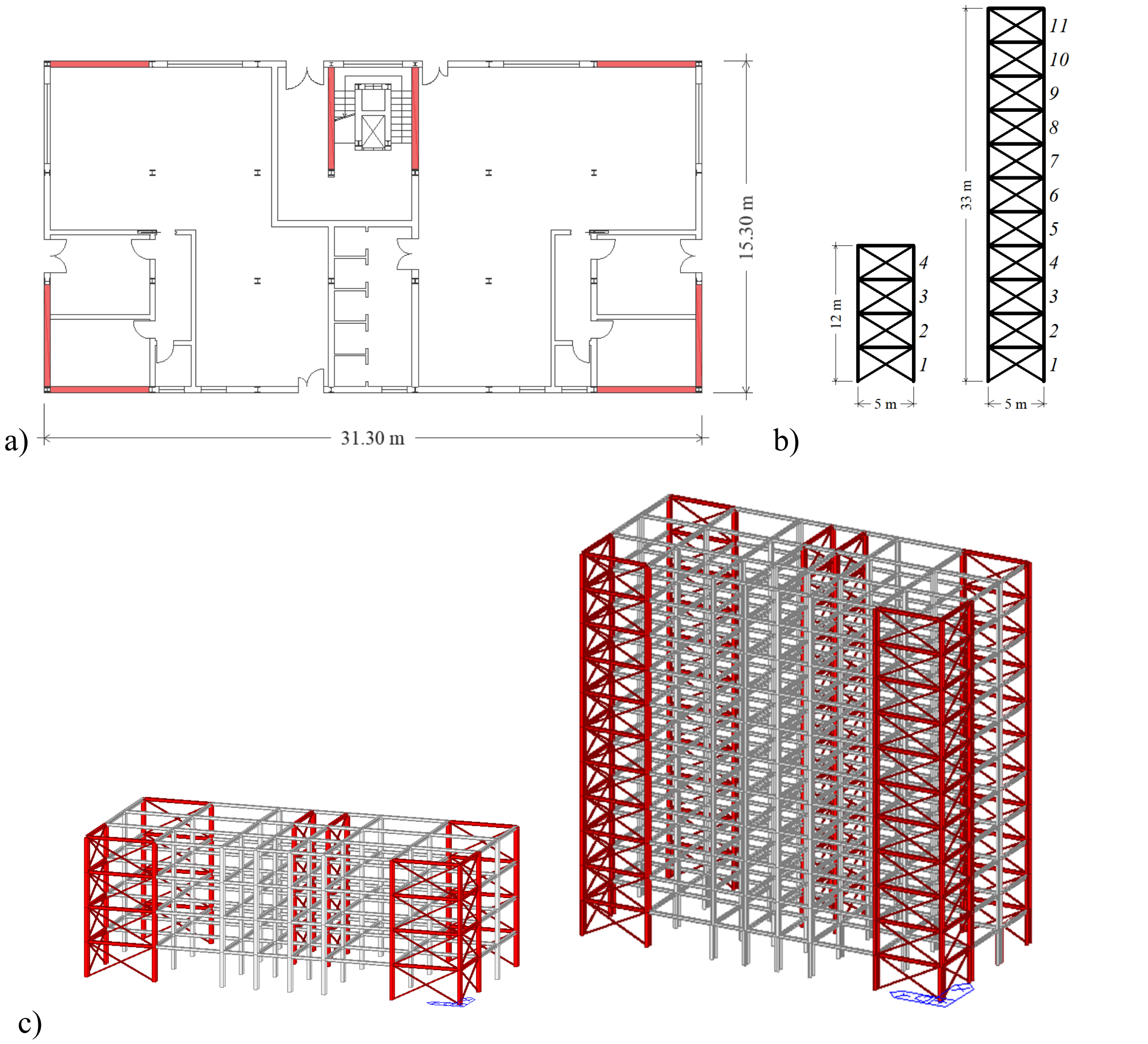

Figure 11: Case study 1: a) building plan with bracing position highlighted in red; b) bracing system for 4 and 11 storeys; c) finite element models for the two buildings.

Table 3: Diagonal elements types considered in the parametric analysis.
Note: Ω is the frequency of the 1st transversal mode of vibration of the diagonals considered as pinned elements; ϑ is the fundamental frequency of the building, which is supposed to be the frequency of load; WR is the working rate.

4 storeys building				
Profile	$\bar{\lambda}$	**Ω (Hz)**	**ϑ (Hz)**	**WR**
HEA180	1.02	17.68	2.347	31.8%
HEA140	1.33	13.69	2.009	44.2%
HEA120	1.56	11.69	1.831	49.3%
HEA100	1.88	9.68	1.697	53.7%
2L90x90x6	1.76	9.41	1.686	53.4%
2L60x60x10	2.74	6.66	1.725	52.4%

11 storeys building				
Profile	$\bar{\lambda}$	**Ω (Hz)**	**ϑ (Hz)**	**WR**
HEA180	1.02	17.68	0.671	32.8%
HEA140	1.33	13.69	0.608	42.3%
HEA120	1.56	11.69	0.571	49.7%
HEA100	1.88	9.68	0.541	57.7%
2L90x90x6	1.76	9.41	0.538	57.6%
2L60x60x10	2.74	6.66	0.547	55.5%

L90x90x7	3.82	4.23	1.345	69.3%
L80x80x10	4.92	3.70	1.470	63.2%
L60x60x5	6.23	2.81	1.006	94.1%

L90x90x7	3.82	4.23	0.450	92.0%
L80x80x10	4.92	3.70	0.484	77.0%
L60x60x10	6.60	2.76	0.436	99.9%

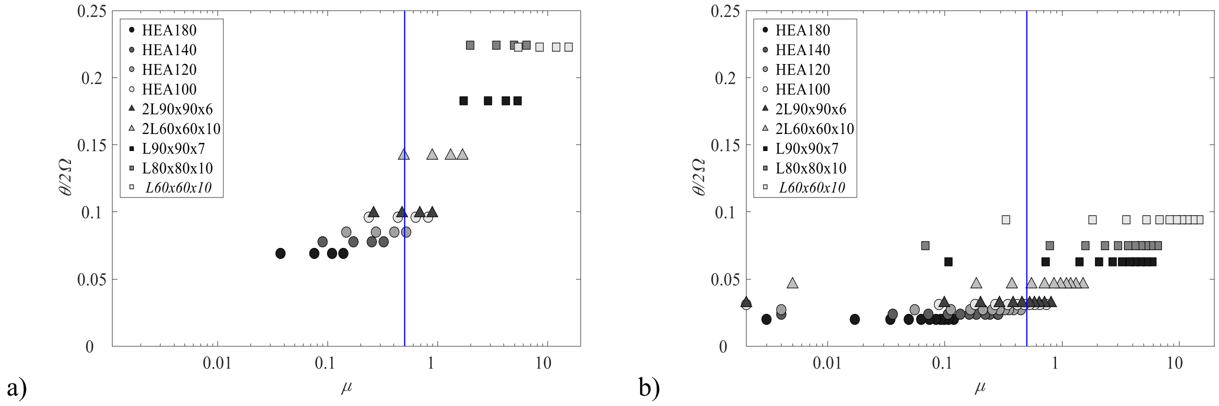

Figure 12: Evaluation of the influence of the profile of the diagonal elements in the μ - $\vartheta/2\Omega$ plane:
a) 4 storeys building; b) 11 storeys building.
Note: abscissa in logarithmic scale for sake of clarity.

In all the considered cases, the points are associated with low frequency ratios, where no stability regions (**Figure 6**) are present beyond the elastic case ($\mu = 0.5$), therefore an axial overload in such diagonal elements is not expected and the design is not affected. It is worth noting that, according to the results presented in the previous section, the design could be affected only for $\vartheta/2\Omega$ greater than 0.18, i.e. only above such value it is possible to find stable regions beyond the static critical load, therefore possibly providing an overload in the compressed elements.

A complete analysis of the bracing systems of the two case studies was carried out considering the HEA100 profile as diagonal elements, because such profile satisfied the Eurocode 8 slenderness requirements. **Table 4** shows the frequency and the modal participation mass of the first two modes of vibrations, obtained from an eigenvalue analysis. **Table 5** reports the values of P_t, i.e. the seismic load, for the first two fundamental modes obtained from the response spectrum analyses and the corresponding point in the μ - $\vartheta/2\Omega$ plane (**Figure 13)** for the bracing system with the highest loading rate. Even the columns of the bracing system are not affected by dynamic instability because they present very low $\vartheta/2\Omega$ ratios, about 0.004, and therefore static instability governs.

Table 4: 1st and 2nd mode of vibration frequency and modal mass.

4 storeys building		
Mode	**Frequency (Hz)**	**Modal mass**
1st	1.866	89.0%
3rd	6.275	8.7%

11 storeys building		
Mode	**Frequency (Hz)**	**Modal mass**
1st	0.602	79.8%
3rd	1.936	13.5%

Table 5: Load (P_t) on the bracing elements and coordinates of the stability plane.

4 storeys		**1st mode**			**2nd mode**	
Level	**P_t (kN)**	**μ**	**$\vartheta/2\Omega$**	**P_t (kN)**	**μ**	**$\vartheta/2\Omega$**
1	347.0	0.815	0.096	26.0	0.061	0.324
2	268.0	0.629	0.096	0.3	0.001	0.324
3	184.0	0.432	0.096	23.0	0.054	0.324
4	101.0	0.237	0.096	26.0	0.061	0.324
11 storeys		**1st mode**			**2nd mode**	
Level	**P_t (kN)**	**μ**	**$\vartheta/2\Omega$**	**P_t (kN)**	**μ**	**$\vartheta/2\Omega$**
1	313.0	0.735	0.031	153.0	0.359	0.100
2	274.0	0.644	0.031	130.0	0.305	0.100
3	247.0	0.580	0.031	90.0	0.211	0.100
4	226.0	0.531	0.031	45.0	0.106	0.100
5	203.0	0.477	0.031	3.3	0.008	0.100
6	177.0	0.416	0.031	46.0	0.108	0.100
7	147.0	0.345	0.031	78.0	0.183	0.100
8	114.0	0.268	0.031	92.0	0.216	0.100
9	77.0	0.181	0.031	87.0	0.204	0.100
10	38.0	0.089	0.031	63.0	0.148	0.100
11	1.0	0.002	0.031	31.0	0.073	0.100

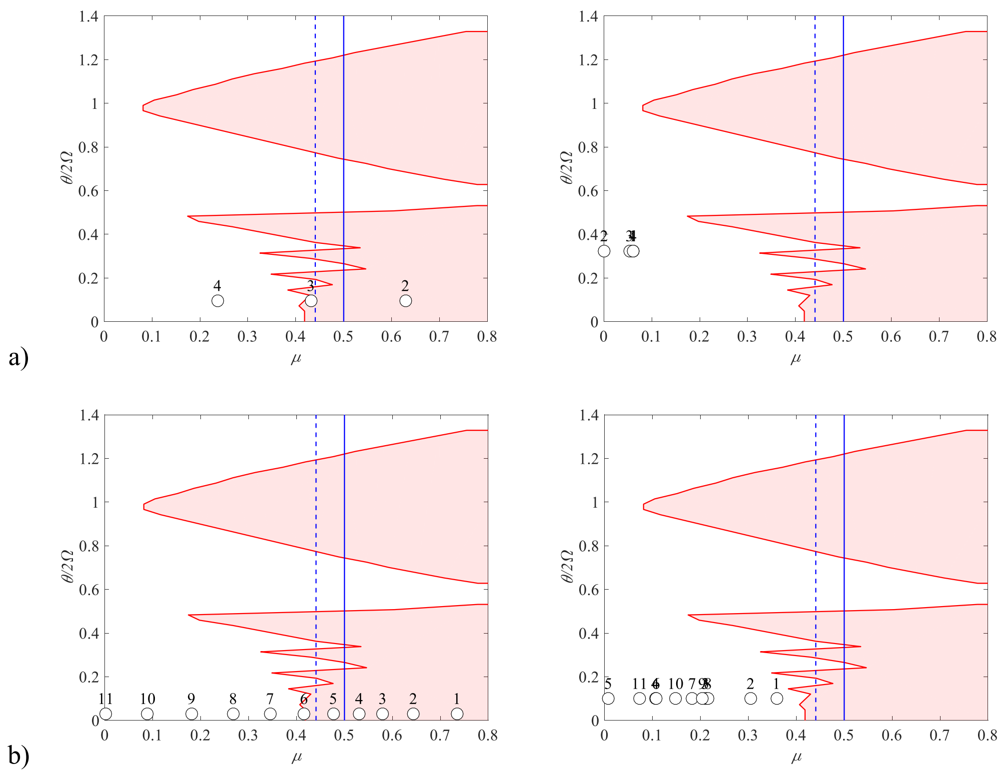

Figure 13: Stability plane for the diagonal elements of Case study 1: a) 4 storeys building; b) 11 storeys building. Note: the number corresponds to the floor level; the shaded region corresponds to the envelope of the instability regions (series B1 and $\xi = 1\%$); 1st and 2nd fundamental mode of vibration on the left and right side, respectively.

4.2. Case study 2: industrial building

The case study shown in **Figure 14** was selected as representative of existing industrial buildings not specifically designed for seismic loading. The building is analysed to highlight possible dynamic instability particularly for the bottom chord of the truss elements in the out-of-plane direction. The columns are made by HEA260 elements, the truss is made by 2 L65x100x11 elements for the top chord, 2 L80x80x8 elements for the bottom chord, and 2 L80x120x10 elements for the diagonal members, the lateral bracing system is made by 2 L80x120x10 elements. The steel grade is S235, the purlin length is 7.5 m and the roof unit mass is 55.8 kg/m^2.

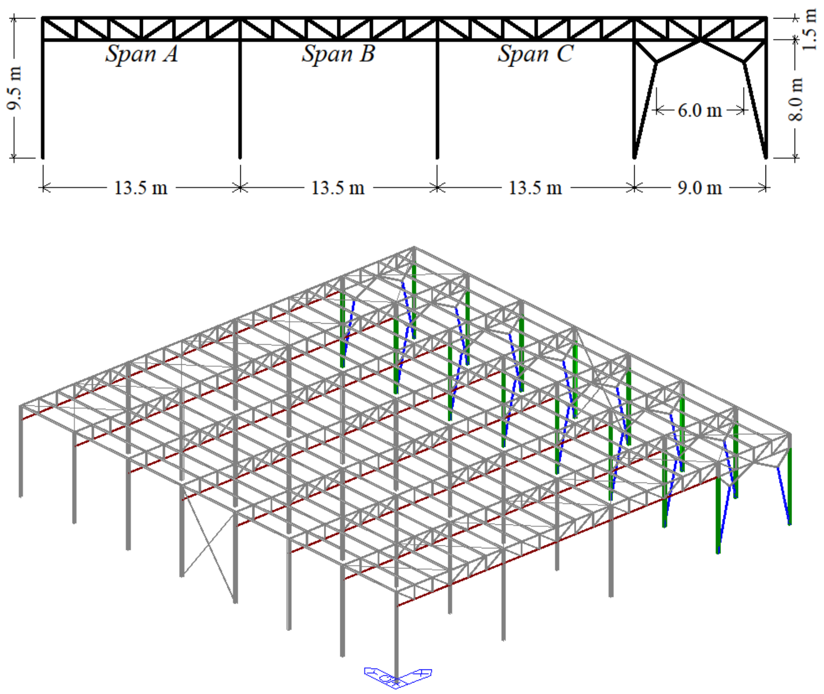

a)

b)

Figure 14: Case study 2: a) building bracing dimensions; b) finite element model.

The frequency of the fundamental mode of vibration, obtained from an eigenvalue analysis, is 3.01Hz. The out-of-plane frequency of vibration of the truss bottom chord is ω = 1.70Hz and the loads obtained from the response spectrum analyses are reported in **Table 6** along with the corresponding points in the stability plot, which are graphically represented in **Figure 15**. Since the chord is composed by various elements, the average axial load is considered herein. From **Figure 15** it is possible to note that the bottom chord of span B and possibly of span C might be affected by out-of-plane dynamic instability. To counteract this phenomenon, it is possible to add additional bracing elements connecting the bottom chords of subsequent frames as shown in **Figure 16**. The resulting points in the stability plots are shown in **Figure 15** with grey circles. Regarding the diagonal elements and the columns of the vertical bracing system, the corresponding points in the instability plot associated with the maximum loaded elements are (0.387; 0.243) and (0.034; 0.183), respectively, which lay outside the region of dynamic instability.

Table 6: Loads acting on the truss bottom chord, frequency (Ω) of the loaded beam, and coordinates of the points in the stability plane

Span	P_0 (kN)	Ω (Hz)	P_t (kN)	μ	$\vartheta/2\Omega$
A	-4.07	1.78	3.9	0.044	0.838
B	6.97	1.54	14.4	0.218	0.968
C	2.43	1.65	8.7	0.116	0.908

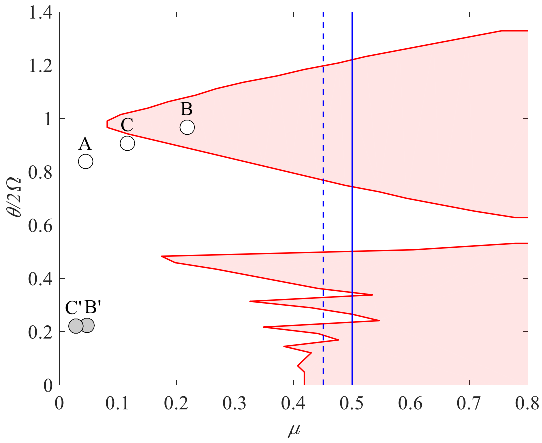

Figure 15: Representation of the points of the lower chords of the truss members in Case study 2 for the 1st mode of vibration in the as-is conditions (in white circles) and after placing additional braces (in grey circles). Note: the letter corresponds to the span. The shaded region corresponds to the envelope of the instability regions obtained from the analyses (series B1 and ξ = 1%).

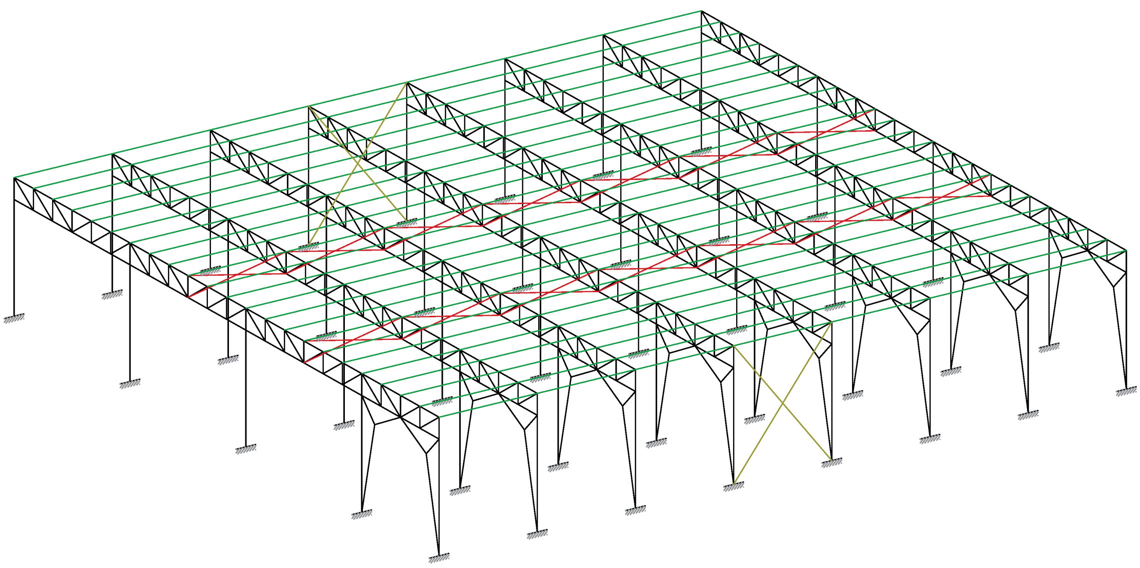

Figure 16: Additional bracing elements (in red) to counteract dynamic instability

5. CONCLUSIONS

This paper investigated the phenomenon of dynamic instability of beams subjected to axial harmonic loading. Starting from the theoretical formulation proposed by Bolotin, a more refined definition of the instability regions was derived. This allowed highlighting conditions under which the beam could become unstable for loading values well below the Euler critical load and conditions under which the beam could be stable for loading values beyond the Euler critical load.

The influence of the geometric and material non-linearity was specifically addressed by performing series of finite element analyses. The results showed that an increase of the initial imperfection leads to an increase of the unstable cases, while for an imperfection amplitude equal to 1/1000 of the beam length, the theoretical results are practically superimposed by the numerical solutions. When the plastic behaviour of the material was introduced, a small reduction of the unstable cases was observed for the 1st instability region, while for the higher order regions an increase of the unstable points was recorded. Such increase leads to a shift to the left of the instability regions (i.e. lower value of the axial load) and it is related to the plastic behaviour of the material, particularly when the lateral deflection demand in the case of elastic material is beyond the displacement associated with yielding in the case of plastic material. It is observed that particularly between the 1st and 2nd instability regions, stable solutions are possible for axial loads higher than the static critical load.

Finally, the possibility of dynamic instability in building type structures due to seismic loading was evaluated. It is possible to account for such phenomenon by means of response spectrum analyses: the variation of the axial load in the elements due to the earthquake is evaluated by considering single modes at the time. This load is considered corresponding to a harmonic excitation with angular frequency equal to the vibration mode. This allows defining a point in the stability plane for each element and verifying its possible instability. It is worth noting that adopting a response spectrum analysis provides results on the safe side because the values of such analysis represent the maximum values experienced by the system during the earthquake.

At this regard two case studies were considered: a cross-braced multi-storey building (with 4 and 11 storeys) designed for seismic actions and an existing single-storey industrial building not designed for seismic actions. The results showed that in the former case the dynamic instability does not occur. In the cross-bracing elements there are no cases where the axial load exceeds the static instability load therefore capacity design is not affected: all the diagonal elements would buckle for loads equal to the static critical loads, therefore without providing an overload in the compressed elements. In addition, in the columns of the bracing system there are no cases where dynamic instability occurs for lower than expected axial loads. This is due to the high frequency of vibration of the single elements compared to the frequency of the fundamental mode of vibrations of the whole building. It is worth noting that only the elements whose points in the stability plot have an ordinate greater than 0.18 could reach loads greater than the static critical loads.

In the latter case, existing industrial buildings not designed to sustain seismic actions, some slender elements, with frequency of vibration compatible with the fundamental frequencies of the building, may experience dynamic instability with possible detrimental effects in the whole building response. For such conditions a retrofit solution based on the introduction of additional bracing elements was proposed. This solution allowed moving the unstable points in the stability plots towards stable regions.

APPENDIX A

The governing equation of the damped case is

$$f'' + 2\varepsilon f' + \Omega^2(1 - 2\mu \cos \vartheta t)f = 0 \tag{A1}$$

This equation could be related to a Mathieu-Hill equation. In fact, performing the substitution

$$f(t) = u(t)\, e^{-\varepsilon t}\,, \tag{A2}$$

Deriving once and twice in respect to time, we obtain

$$\begin{aligned} f'(t) &= u'(t)\, e^{-\varepsilon t} - \varepsilon\, u(t)\, e^{-\varepsilon t} \\ f''(t) &= u''(t)\, e^{-\varepsilon t} - 2\varepsilon\, u'(t) e^{-\varepsilon t} + \varepsilon^2\, u(t)\, e^{-\varepsilon t} \end{aligned} \tag{A3}$$

Substituting such equations into Eq. (A1):

$$\begin{aligned} &u''(t)\, e^{-\varepsilon t} - 2\varepsilon\, u'(t) e^{-\varepsilon t} + \varepsilon^2\, u(t)\, e^{-\varepsilon t} + 2\varepsilon u'(t)\, e^{-\varepsilon t} \\ &-\varepsilon\, u(t)\, e^{-\varepsilon t} + \Omega^2(1 - 2\mu \cos \vartheta t)\, u(t)\, e^{-\varepsilon t} = 0 \end{aligned} \tag{A4}$$

and simplifying

$$u''(t)\, e^{-\varepsilon t} + (-\varepsilon^2 + \Omega^2 - 2\mu\, \Omega^2 \cos \vartheta t)\, u(t)\, e^{-\varepsilon t} = 0 \tag{A5}$$

Multiplying by $e^{\varepsilon t}$ and collecting the term Ω^2:

$$u''(t) + \Omega^2 \left(1 - \frac{\varepsilon^2}{\Omega^2} - 2\mu \cos \vartheta t\right) u(t) = 0 \tag{A6}$$

To obtain the general form of the Mathieu-Hill equation, we substitute

$$u(t) = y\left(\frac{\vartheta t}{2}\right) \tag{A7}$$

By deriving twice, we obtain

$$u''(t) = \frac{\vartheta^2}{4} y''\left(\frac{\vartheta t}{2}\right) \tag{A8}$$

Substituting Eq. (A7) and Eq. (A8) in Eq. (A6), we obtain

$$\frac{\vartheta^2}{4} y''\left(\frac{\vartheta t}{2}\right) + \Omega^2 \left(1 - \frac{\varepsilon^2}{\Omega^2} - 2\mu \cos \vartheta t\right) y\left(\frac{\vartheta t}{2}\right) = 0 \tag{A9}$$

Finally, replacing the independent variable $x = \vartheta t/2$ and multiplying by $4/\vartheta^2$, we obtain the general form of the Mathieu-Hill equation:

$$y''(x) + \frac{4\Omega^2}{\vartheta^2}\left(1 - \frac{\varepsilon^2}{\Omega^2} - 2\mu \cos(2x)\right) y(x) = 0 \tag{A10}$$

Since this equation is related to a Mathieu-Hill equation, the solution follows the mathematical properties of such type of equations [20]. The boundaries of the odd and even instability regions are obtained from searching periodic solutions of period *2T* and *T*, respectively:

$$f(t) = \sum_{k=1,3,5}^{\infty} \left(a_k \sin\frac{k\vartheta t}{2} + b_k \cos\frac{k\vartheta t}{2}\right) \tag{A11}$$

$$f(t) = b_0 + \sum_{k=2,4,6}^{\infty} \left(a_k \sin\frac{k\vartheta t}{2} + b_k \cos\frac{k\vartheta t}{2}\right) \tag{A12}$$

By replacing one at a time Eq. (A11) and Eq. (A12) into Eq. (A10), the following systems of equations is obtained, respectively:

$$\begin{cases} \left(1+\mu-\frac{\vartheta^2}{4\Omega^2}\right)a_1-\mu a_3-\frac{\Delta}{\pi}\frac{\vartheta}{2\Omega}b_1=0 \\ \left(1-\mu-\frac{\vartheta^2}{4\Omega^2}\right)b_1-\mu b_3+\frac{\Delta}{\pi}\frac{\vartheta}{2\Omega}a_1=0 \\ \cdots \\ \left(1-\frac{k^2\vartheta^2}{4\Omega^2}\right)a_k-\mu(a_{k-2}+a_{k+2})-\frac{\Delta}{\pi}\frac{k\vartheta}{2\Omega}b_k=0 \qquad (k=3,5,7,\ldots) \\ \left(1-\frac{k^2\vartheta^2}{4\Omega^2}\right)b_k-\mu(b_{k-2}+b_{k+2})+\frac{\Delta}{\pi}\frac{k\vartheta}{2\Omega}a_k=0 \qquad (k=3,5,7,\ldots) \end{cases} \tag{A13}$$

$$\begin{cases} b_0-\mu b_2=0 \\ \left(1-\frac{\vartheta^2}{\Omega^2}\right)a_2-\mu a_4-\frac{\Delta}{\pi}\frac{\vartheta}{\Omega}b_2=0 \\ \left(1-\frac{\vartheta^2}{\Omega^2}\right)b_2-\mu(2b_0+b_4)+\frac{\Delta}{\pi}\frac{\vartheta}{\Omega}a_2=0 \\ \cdots \\ \left(1-\frac{k^2\vartheta^2}{4\Omega^2}\right)a_k-\mu(a_{k-2}+a_{k+2})-\frac{\Delta}{\pi}\frac{k\vartheta}{2\Omega}b_k=0 \qquad (k=4,6,8,\ldots) \\ \left(1-\frac{k^2\vartheta^2}{4\Omega^2}\right)b_k-\mu(b_{k-2}+b_{k+2})+\frac{\Delta}{\pi}\frac{k\vartheta}{2\Omega}a_k=0 \qquad (k=4,6,8,\ldots) \end{cases} \tag{A14}$$

where Δ is defined as:

$$\Delta = 2\pi\xi \tag{A15}$$

In order to obtain the non-trivial solution of such systems, the determinant of the matrix constructed with the coefficients of the terms a_k and b_k must be zero. In this way and through some simplifications (i.e. by considering only 2x2 systems of equations), Bolotin [13] determined three regions of dynamic instability, as represented in **Figure A1**, which are included between the boundaries defined by the following equations:

$$\frac{\vartheta}{2\Omega}=\sqrt{1-0.5(2\xi)^2\pm\sqrt{\mu^2-(2\xi)^2+0.25(2\xi)^4}} \tag{A16}$$

$$\frac{\vartheta}{2\Omega}=\frac{1}{2}\sqrt{1-\mu^2\pm\sqrt{\mu^4-(2\xi)^2(1-\mu^2)}} \tag{A17}$$

$$\frac{\vartheta}{2\Omega}=\frac{1}{3}\sqrt{1-\frac{8/9\mu^2\pm\sqrt{\mu^6-(2\xi)^2(64/81-2/3\mu^2)}}{64/81-\mu^2}} \tag{A18}$$

It is worth noting that stability regions for $\mu > 0.5$ define conditions in which stability is guaranteed for axial loads exceeding the Euler critical load.

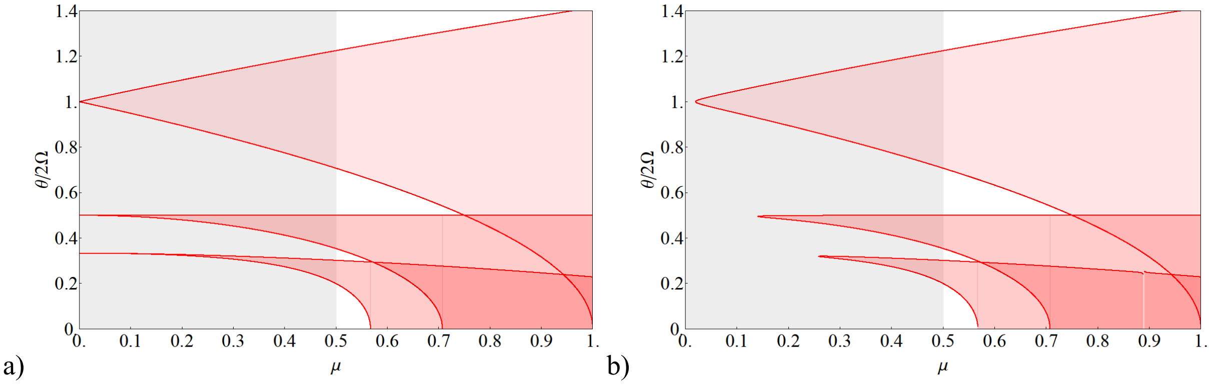

Figure A1: Regions of dynamic instability determined by Bolotin [13]: a) non-damped case; b) damped case ($\xi = 1\%$). Note: the original region investigated by Bolotin corresponds to the shaded area.

To refine the results obtained by Bolotin [13], the systems in Eq. (A13) and Eq. (A14) were extended to reach a matrix size 8x8 and 7x7 respectively; in this way, 7 instability regions were derived. It is worth noting that the greater the number of terms considered in Eq. (A11) and Eq. (A12), the greater the size of the matrix to be solved and the greater the number of instability regions and the accuracy of their boundaries. The matrix obtained from the system in Eq. (A13) and Eq. (A14) become respectively:

$$\begin{bmatrix} 1-\frac{49\vartheta^2}{4\Omega^2} & -\mu & 0 & 0 & 0 & 0 & 0 & -\frac{\Delta}{\pi}\frac{7\vartheta}{2\Omega} \\ -\mu & 1-\frac{25\vartheta^2}{4\Omega^2} & -\mu & 0 & 0 & 0 & -\frac{\Delta}{\pi}\frac{5\vartheta}{2\Omega} & 0 \\ 0 & -\mu & 1-\frac{9\vartheta^2}{4\Omega^2} & -\mu & 0 & -\frac{\Delta}{\pi}\frac{3\vartheta}{2\Omega} & 0 & 0 \\ 0 & 0 & -\mu & 1+\mu-\frac{\vartheta^2}{4\Omega^2} & -\frac{\Delta}{\pi}\frac{\vartheta}{2\Omega} & 0 & 0 & 0 \\ 0 & 0 & 0 & \frac{\Delta}{\pi}\frac{\vartheta}{2\Omega} & 1-\mu-\frac{\vartheta^2}{4\Omega^2} & -\mu & 0 & 0 \\ 0 & 0 & \frac{\Delta}{\pi}\frac{3\vartheta}{2\Omega} & 0 & -\mu & 1-\frac{9\vartheta^2}{4\Omega^2} & -\mu & 0 \\ 0 & \frac{\Delta}{\pi}\frac{5\vartheta}{2\Omega} & 0 & 0 & 0 & -\mu & 1-\frac{25\vartheta^2}{4\Omega^2} & -\mu \\ \frac{\Delta}{\pi}\frac{7\vartheta}{2\Omega} & 0 & 0 & 0 & 0 & 0 & -\mu & 1-\frac{49\vartheta^2}{4\Omega^2} \end{bmatrix} \tag{A19}$$

$$\begin{bmatrix} 1-\frac{36\vartheta^2}{4\Omega^2} & -\mu & 0 & 0 & 0 & 0 & -\frac{\Delta}{\pi}\frac{6\vartheta}{2\Omega} \\ -\mu & 1-\frac{16\vartheta^2}{4\Omega^2} & -\mu & 0 & 0 & -\frac{\Delta}{\pi}\frac{4\vartheta}{2\Omega} & 0 \\ 0 & -\mu & 1-\frac{4\vartheta^2}{4\Omega^2} & 0 & -\frac{\Delta}{\pi}\frac{2\vartheta}{2\Omega} & 0 & 0 \\ 0 & 0 & 0 & 1 & -\mu & 0 & 0 \\ 0 & 0 & \frac{\Delta}{\pi}\frac{2\vartheta}{2\Omega} & -2\mu & 1-\frac{4\vartheta^2}{4\Omega^2} & -\mu & 0 \\ 0 & \frac{\Delta}{\pi}\frac{4\vartheta}{2\Omega} & 0 & 0 & -\mu & 1-\frac{16\vartheta^2}{4\Omega^2} & -\mu \\ \frac{\Delta}{\pi}\frac{6\vartheta}{2\Omega} & 0 & 0 & 0 & 0 & -\mu & 1-\frac{36\vartheta^2}{4\Omega^2} \end{bmatrix} \tag{A20}$$

APPENDIX B

After evaluating the regions of dynamic instability, a conservative "no-instability region" for the elastic case was identified. In this region, the behaviour of the axially loaded beam is stable. This region is herein approximately defined by piecewise linear functions between known reference points. The first 2 points (abscissa and ordinate) are taken from Bolotin [13]:

$$\mu = \sqrt[k]{\frac{\Delta}{\pi}} = \sqrt[k]{2\xi}\;; \quad \frac{\vartheta}{2\Omega} = \frac{1}{k} \tag{B1}$$

where k is the number of the instability region, herein 1 and 2.

Three possible conditions are distinguished as a function of the damping factor.

Case 1, $\xi < 3\%$. The no-instability region is bounded by a broken line passing through points A, B and C (**Figure B1a, b**). Where points A and B correspond to the origin points of the first 2 instability regions, Eq. (21), and point C, of coordinates (0.5; 0), corresponds to the achievement of the Euler critical load in the static case.

Case 2, $\xi = 3\%$. An additional point D, of coordinates (0.5; 0.125), is introduced in addition to the aforementioned points A, B and C, since the value of the abscissa of the regions higher than the 7th is approximately equal to 0.5. Consequently, the DC segment will be a vertical segment (**Figure B1c**).

Case 3, $\xi > 3\%$. The point A, B, and C are the same as in the previous cases. The point D has an ordinate equal to 0.125, while the abscissa is determined by a linear regression relating μ to ξ:

$$\mu = 0.45 + 1.59\,\xi \tag{B2}$$

The corresponding no-instability region is shown in **Figure B1d**.

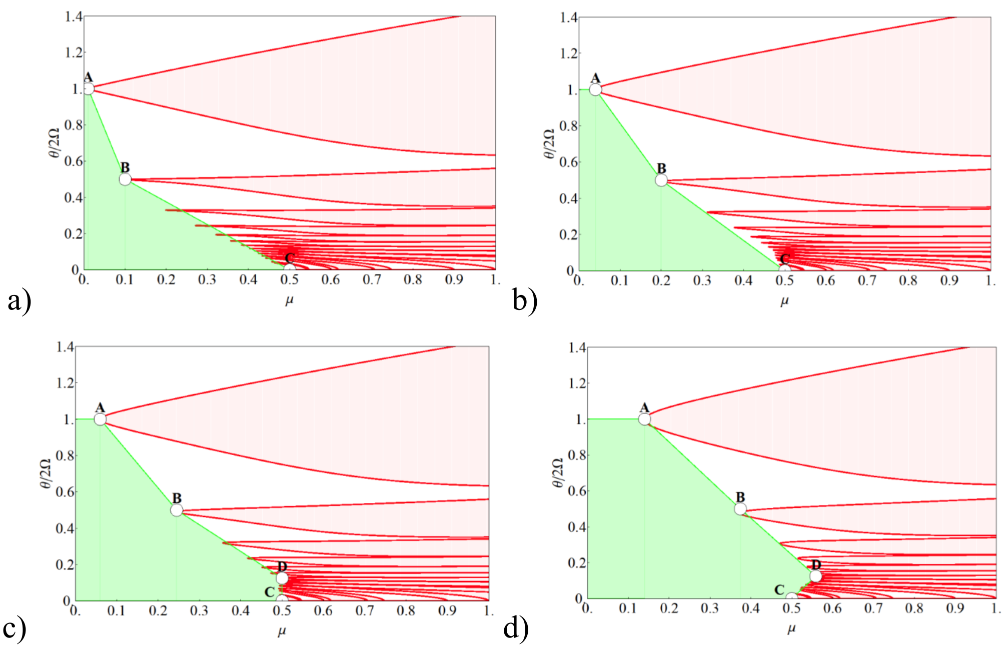

Figure B1: No-instability regions: a) $\xi = 0.5\%$; b) $\xi = 2.0\%$; c) $\xi = 3.0\%$; d) $\xi = 7.0\%$.

APPENDIX C

The results of the analyses of model A, model B and model C with relative damping equal to 3% are reported in **Figure C1, Figure C2** and **Figure C3** respectively.

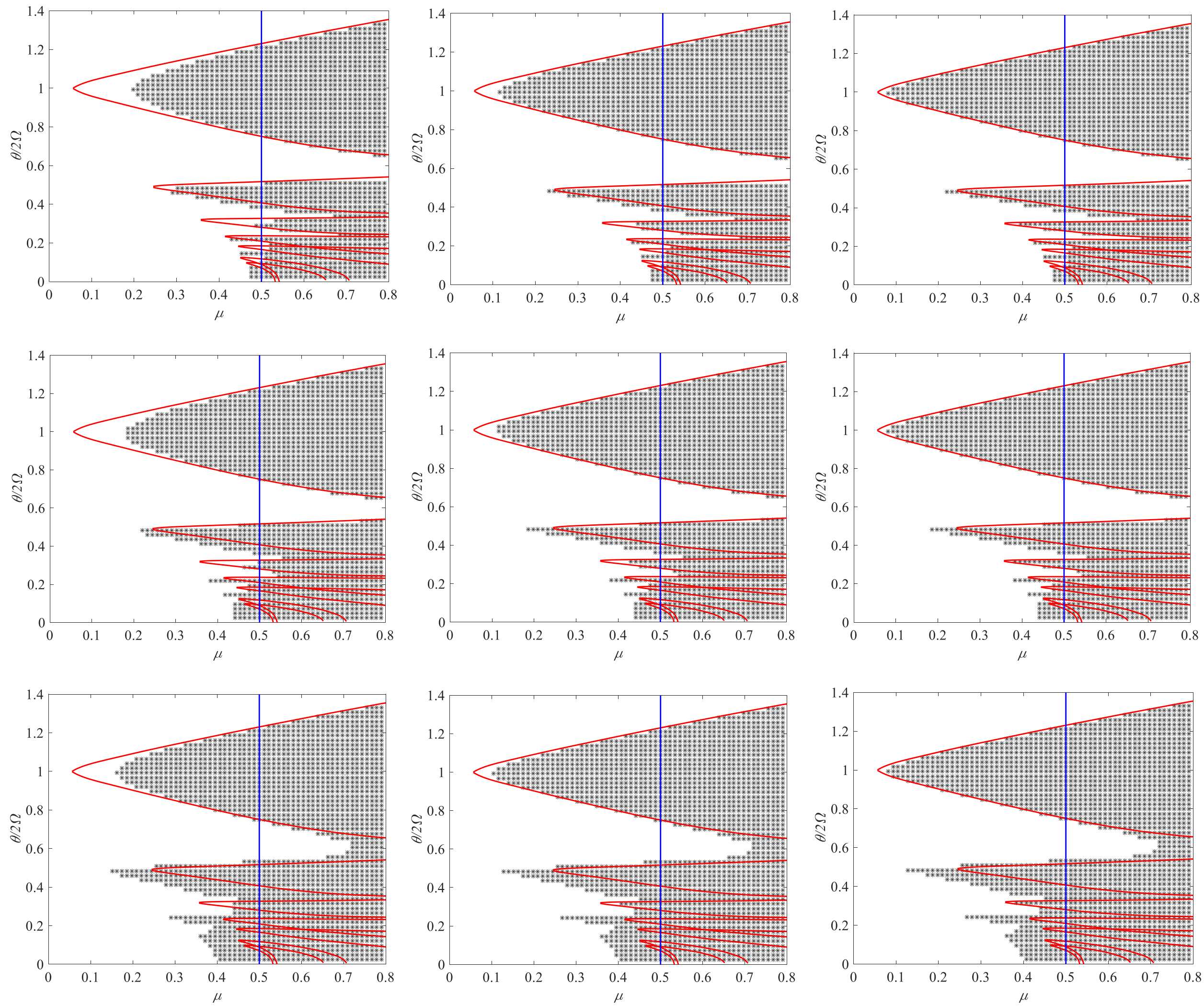

Figure C1: Results of model A with damping equal to 3%: investigation of geometric non-linearity (series A1, A2, and A3 from top to bottom) for different durations of the analysis time (1s, 3s, and 10s from left to right).

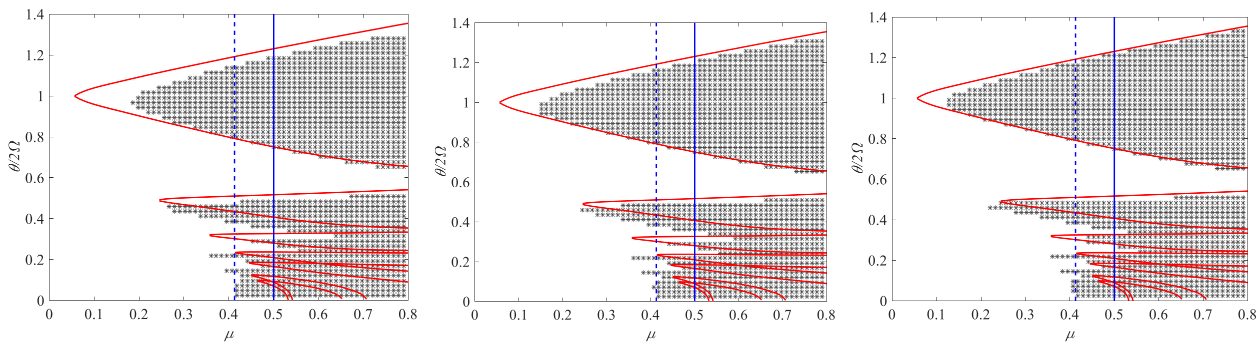

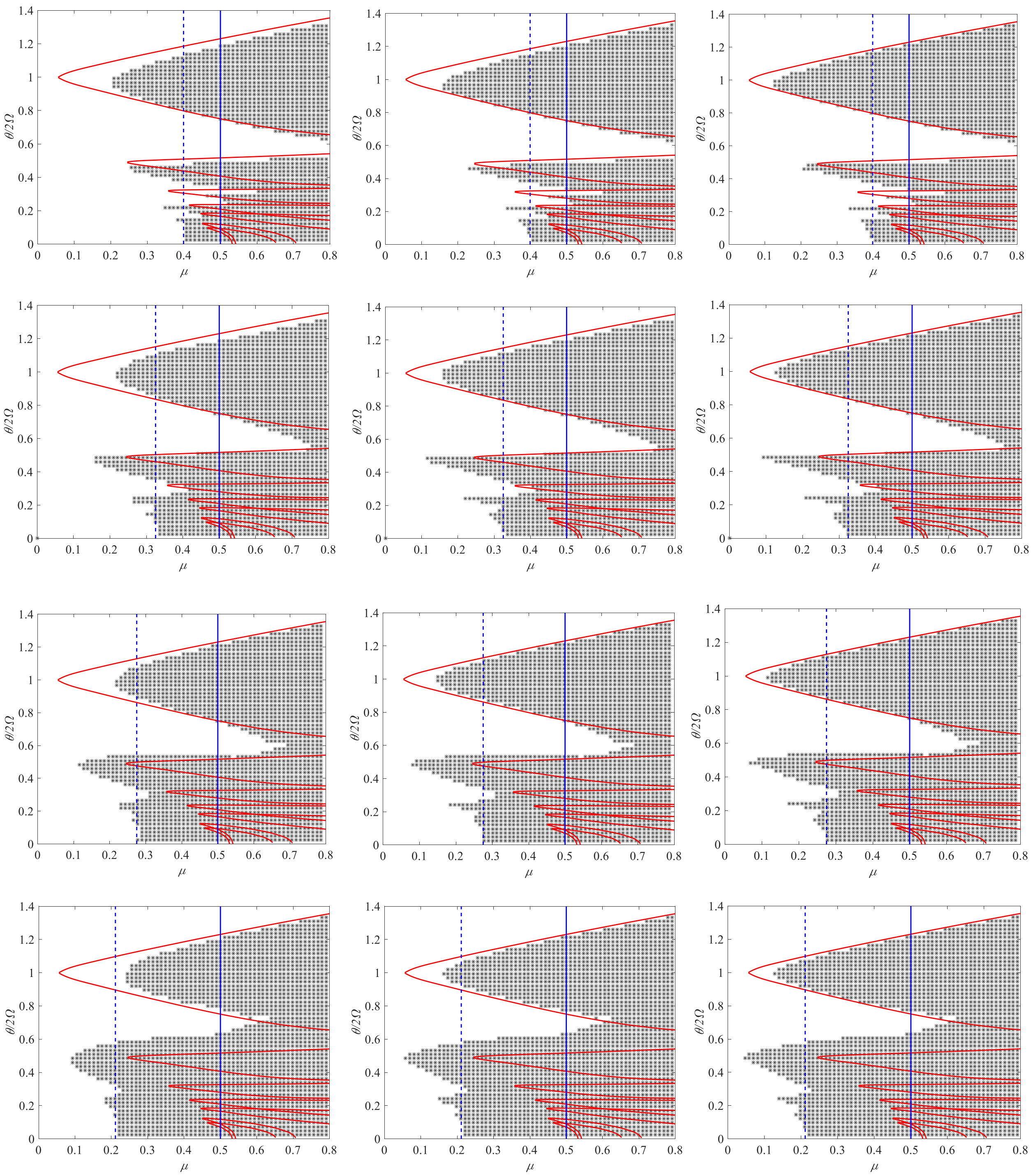

Figure C2: Results of model B with damping equal to 3%: investigation of material non-linearity (series B1, B2, B3, B4, and B5 from top to bottom) for different durations of the analysis time (1s, 3s, and 10s from left to right).

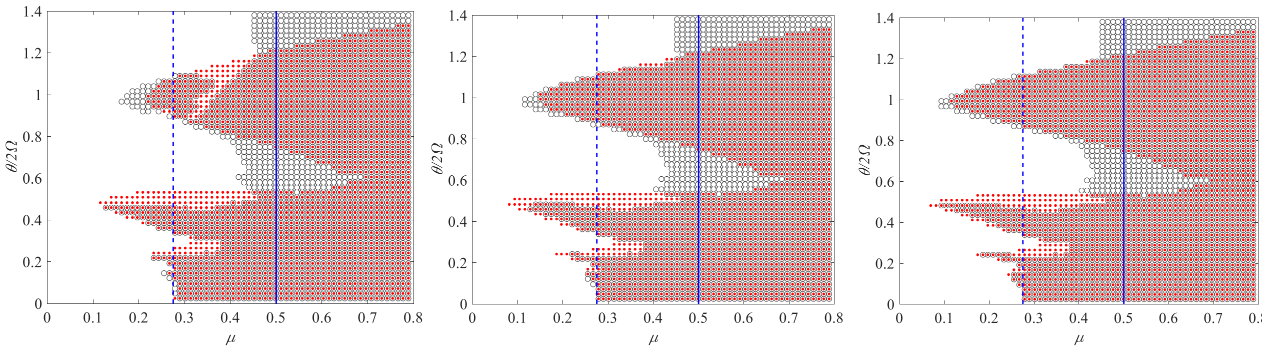

Figure C3: Results of model C with damping equal to 3%: investigation of the influence of the slenderness ratio (series C1) for different durations of the analysis time (1s, 3s, and 10s from left to right).

Note: the empty and filled circles are the unstable points of series C1 and B4 respectively.

Figure C4 shows a close up of the results in the plane (μ; $\vartheta/2\Omega$) between (0; 0) and (0.5;0.6). In that case the designer could directly enter the provided graphs with the (μ; $\vartheta/2\Omega$) point corresponding to a specific element and loading conditions and determine the possibility of dynamic instability. The refinement is associated with an initial imperfection with amplitude $A_{imp} = L/500$ and both for a relative damping $\xi = 1\%$ and for $\xi = 3\%$. These results can be seen as an extension of what presented in Appendix B for the elastic case.

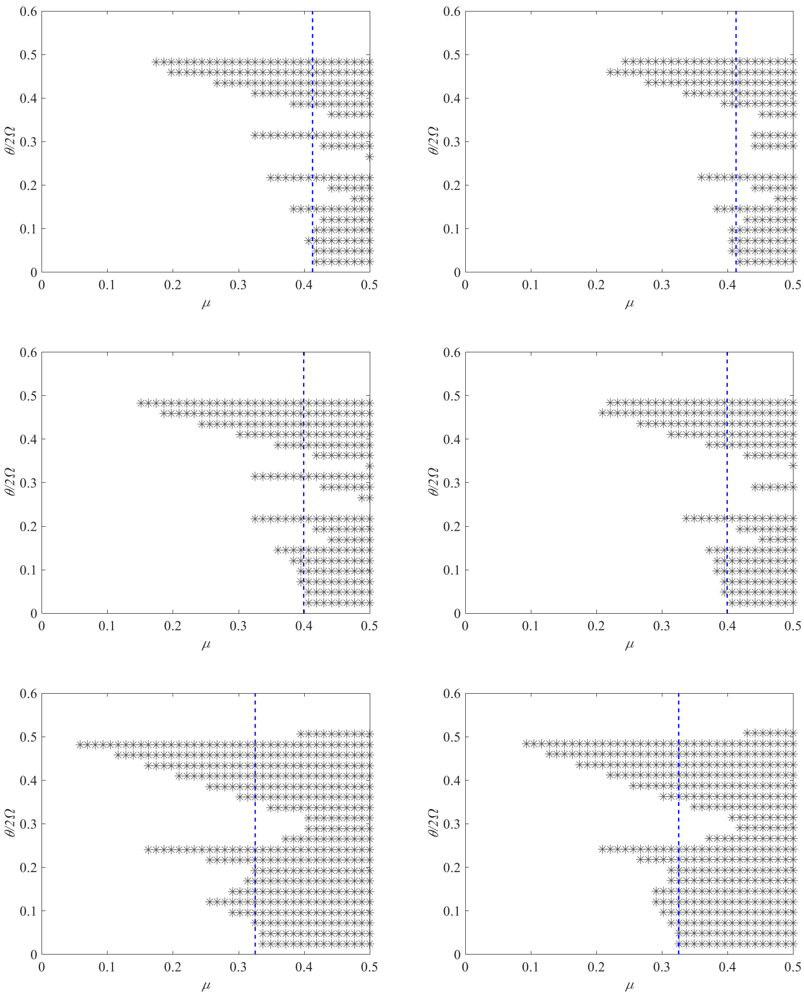

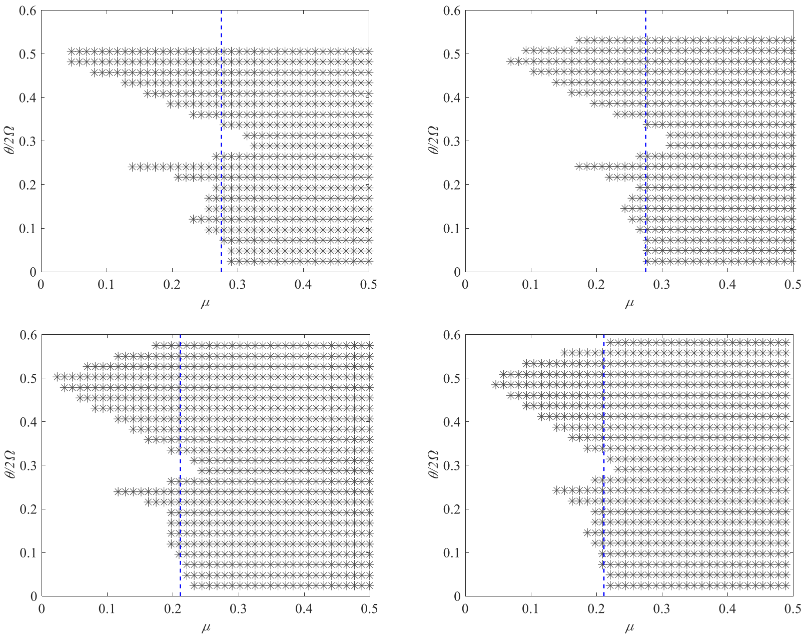

Figure C4: Investigation of the influence of geometry and material non-linearity on the no-instability region varying the P_0 / P_{pl} ratio (0.0%, 16.3%, 60.6%, 74.2% and 84.5% from top to bottom) for different values of relative damping (1% on the left and 3% on the right).

Acknowledgements

The analytical support of prof. G. Gigante, University of Bergamo, in dealing with the Mathieu-Hill equations is gratefully acknowledged.

REFERENCES

[1] Timoshenko S.P., Gere J.M., Young D.H. (1963). Theory of elastic stability, McGraw-Hill.

[2] Southwell R.V. (1931). On the analysis of experimental observations in problems of elastic stability. Proceedings of the Royal Society of London, 135(828):601-616.

[3] Ericksen J.L. (1966). A thermo-kinetic view of elastic stability theory. International Journal of Solids and Structures, 2(4):573-580.

[4] Chajes A. (1974). Principles of structural stability theory. Prentice-Hall.

[5] Atanackovic T.M. (1997). Stability theory of elastic rods. World Scientific Publishing, UK.

[6] Holden J.T. (1964). Estimation of critical loads in elastic stability theory. Archive for Rational Mechanics and Analysis, 17(3):171–183.

[7] Potier-Ferry M. (1982). On the mathematical foundations of elastic stability theory. Archive for Rational Mechanics and Analysis, 78(1):55–72.

[8] Wu G.Y., Shih Y.S. (2006). Analysis of dynamic instability for arbitrarily laminated skew plates. Journal of Sound and Vibration, 292(1-2):315-340.

[9] Hutt J.M., Salam A.E. (1971). Dynamic instability of plates by finite element method. ASCE Journal of Engineering Mechanics, 3:879-899.
[10] Srinivasan R.S., Chellapandi P. (1986). Dynamic stability of rectangular laminated composite plates. Computers & Structures, 24:233-238.
[11] Chen L.W., Yang J.Y. (1990). Dynamic stability of laminated composite plates by the finite element method. Computers & Structures, 36:845–851.
[12] Srivastava A.K.L., Datta P.K., Sheikh A.H. (2003). Dynamic instability of stiffened plates subjected to non-uniform harmonic in-plane edge loading. Journal of Sound and Vibration, 262(5):1171-1189.
[13] Bolotin V.V. (1964). The dynamic stability of elastic systems. Holden-Day Inc, San Francisco, USA.
[14] Lavrentiev M.A., Ishlinsky A. Y. (1949). Dynamic forms of loss of stability of elastic systems (in Russian). Doklady (Transactions) of the USSR Academy of Sciences 64:776-82.
[15] Belyaev A.K., Ilin D.N., Morozov N.F. (2013). Stability of transverse vibration of rod under longitudinal step-wise loading. Journal of Physics: Conference Series, 451 (2013) 012023.
[16] Huang Y-Q, Lu H-W, Fu J-Y, Liu A-R, Gu M. (2014). Dynamic stability of Euler beams under axial unsteady wind force. Mathematical Problems in Engineering, Vol. 2014, article ID 434868.
[17] Kazemzadeh Azad S., Topkaya C., Bybordiani M. (2017). Dynamic buckling of braced in concentrically braced frames. Earthquake Engineering and Structural Dynamics, 47(3):613-633.
[18] Briseghella L., Majorana C.E., Pellegrino C. (1998). Dynamic stability of elastic structures: a finite element approach. Computers and Structures, 69(1):11-25.
[19] Mathieu E. (1868). Memoire sur le mouvement vibratoire d'une membrane de forme elliptique. Journal des Mathematiques Pures et Appliquees, 13: 137-203.
[20] McLachlan N.W. (1947). Theory and Application of Mathieu Functions, Oxford University Press, UK.
[21] ABAQUS 6.14 (2014), Dassault Systèmes Simulia Corp.
[22] Papazafeiropoulos G., Muñiz-Calvente M., Martínez-Pañeda E. (2017). Abaqus2Matlab: a suitable tool for finite element post-processing. Advances in Engineering Software. 105:9-16.
[23] MATLAB R2018a, The MathWorks, Inc.
[24] MidasGEN 2018, MIDAS Information Technologies Co. Ltd.

[25] EN 1998-1:2005, Eurocode 8: Design of structures for earthquake resistance - Part 1: General rules, seismic actions and rules for buildings, European Committee for Standardization, Brussels, Belgium.

[26] Chopra AK, 2012, “Dynamics of Structures: Theory and Applications to Earthquake Engineering”, Prentice-hall, New Jersey, USA.